THE ASTROPHYSICAL JOURNAL, 519:762–770, 1999 July 10
© 1999. The American Astronomical Society. All rights reserved. Printed in U.S.A.

MULTIWAVELENGTH OBSERVATIONS OF GX 339−4 IN 1996. I. DAILY LIGHT CURVES AND X-RAY AND GAMMA-RAY SPECTROSCOPY

I. A. SMITH,[1] E. P. LIANG,[1] D. LIN,[1] M. MOSS,[1,2] A. CRIDER,[1] R. P. FENDER,[3] PH. DUROUCHOUX,[4] S. CORBEL,[4] AND R. SOOD[5]

Received 1998 July 7; accepted 1999 February 12

ABSTRACT

As part of our multiwavelength campaign of GX 339−4 observations in 1996, we present our radio, X-ray, and gamma-ray observations made in July, when the source was in a hard state (=soft X-ray low state). The radio observations were made at the time when there was a possible radio jet. We show that the radio spectrum was flat and significantly variable and that the radio spectral shape and amplitude at this time were not anomalous for this source. Daily light curves from our pointed observation on July 9–23 using the Oriented Scintillation Spectrometer Experiment (OSSE) on the *Compton Gamma-Ray Observatory* (*CGRO*), from the Burst and Transient Source Experiment (BATSE) on *CGRO*, and from the All-Sky Monitor on the *Rossi X-Ray Timing Explorer* (*RXTE*) also show that there was no significant change in the X-ray and gamma-ray flux or hardness during the time when the possible radio jet–like feature was seen. The higher energy portion of our pointed *RXTE* observation made on July 26 can be equally well fitted using simple power law times exponential (PLE) and Sunyaev-Titarchuk (ST) functions. An additional soft component is required, as well as a broad emission feature centered on ∼6.4 keV. This may be an iron line that is broadened by orbital Doppler motions and/or scattering off a hot medium. Its equivalent width is ∼600 eV. Our simplistic continuum fitting does not require an extra reflection component. Both a PLE and an ST model also fit our OSSE spectrum on its own. Although the observations are not quite simultaneous, combining the *RXTE* and *CGRO* spectra we find that the PLE model easily fits the joint spectrum. However, the ST model drops off too rapidly with increasing energies to give an acceptable joint fit.

Subject headings: accretion, accretion disks — binaries: close — black hole physics — stars: individual (GX 339−4) — X-rays: stars

1. INTRODUCTION AND OVERVIEW

Most Galactic black hole candidates exhibit at least two distinct spectral states (see Liang & Narayan 1997; Liang 1998; Poutanen 1998 for reviews). In the hard state (=soft X-ray low state), the spectrum from ∼keV to a few hundred keV is a hard power law (photon index 1.5 ± 0.5) with an exponential cutoff. This can be interpreted as inverse Comptonization of soft photons. In the soft state (often, but not always, accompanied by the soft X-ray high state), the spectrum above ∼10 keV is a steep power law (photon index greater than 2.2) with no detectable cutoff out to ∼MeV. This multistate behavior is seen in both persistent sources (e.g., Cyg X-1) and transient black hole X-ray novae (e.g., GRS 1009−45). GX 339−4 is unusual in that it is a persistent source, being detected by X-ray telescopes most of the time, but it also has nova-like flaring states.

In 1996, we performed a series of multiwavelength observations of GX 339−4 when it was in a hard state (=soft X-ray low state). This paper is one of a series that describes the results of that campaign. In Paper II (Smith & Liang 1999) we discuss the rapid X-ray timing variability in an observation made by the *Rossi X-Ray Timing Explorer* (*RXTE*) on 1996 July 26 UT. In Paper III (Smith, Filippenko, & Leonard 1999) we discuss our Keck spectroscopy performed on 1996 May 12 UT. These papers expand significantly on our preliminary analyses (Smith et al. 1997a, 1997b).

We start this paper by presenting in § 2 the radio spectra from 1996 July, taken when there was a possible radio jet (Fender et al. 1997). We show that the radio spectrum is flat and significantly variable and that the spectral shape and amplitude were not unusual for the source at that time. In § 3 we discuss the observing and data analysis details for our pointed observation on 1996 July 9–23 using the Oriented Scintillation Spectrometer Experiment (OSSE) on the *Compton Gamma-Ray Observatory* (*CGRO*). In § 4 we show the daily X-ray and gamma-ray light curves from 1996 July. In addition to our OSSE results, we show the data obtained by the All-Sky Monitor (ASM) on *RXTE* and by the Burst and Transient Source Experiment (BATSE) on *CGRO* using the Earth-occultation technique. The soft X-ray flux during our observations was very low, and the spectrum was very hard. However, unlike at the time of our Keck observation on 1996 May 12, the source was significantly detected during most of the month. Most importantly, there was no significant change in the higher energy emission during the time when the radio jet–like feature was seen. In § 5, we present the OSSE spectrum and fit it with simple power law times exponential (PLE) and Sunyaev-Titarchuk (ST; Sunyaev & Titarchuk 1980) functions. They both give equally good fits to the OSSE data alone. In § 6, we discuss the observing and data analysis details for the 1996 July 26 *RXTE* observation. In § 7 we present the X-ray spectros-

[1] Department of Space Physics and Astronomy, Rice University, MS 108, 6100 South Main Street, Houston, TX 77005-1892.
[2] Currently at McDonnell-Douglas, St. Louis, MO.
[3] Astronomical Institute "Anton Pannekoek," Center for High-Energy Astrophysics, University of Amsterdam, Kruislaan 403, 1098 SJ Amsterdam, The Netherlands.
[4] DAPNIA, Service d'Astrophysique, CE Saclay, 91191 Gif sur Yvette Cedex, France.
[5] School of Physics, ADFA, Northcott Drive, Canberra ACT 2600, Australia.

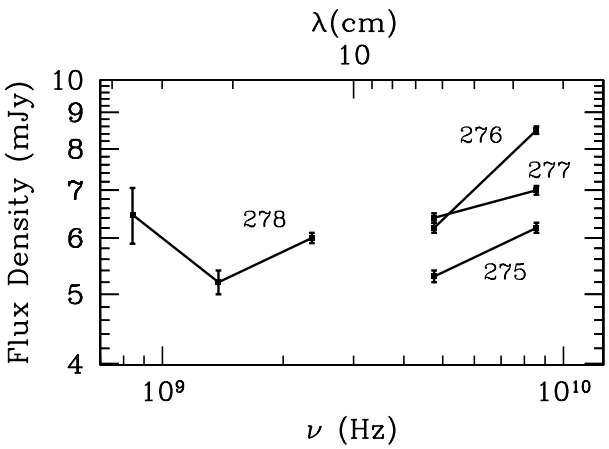

FIG. 1.—Daily radio spectra in 1996 July. All the data points are from ATCA, except the one at 843 MHz, which is from MOST. Labels are MJD − 50,000; 1996 July 11 is MJD 50,275.

copy from the *RXTE* observation. Both a PLE and an ST model can explain the *RXTE* data alone. An additional soft component is required, as well as a *broad* emission feature centered on ∼6.4 keV. This may be an iron line that is broadened by orbital Doppler motions and/or scattering off a hot medium. Its equivalent width is ∼600 eV. Combining the *RXTE* and *CGRO* spectra, we finally show in § 8 that the PLE model easily fits the joint spectrum, but that the ST model does not. In Böttcher, Liang, & Smith (1998) we use the GX 339−4 spectral data to test our detailed self-consistent accretion disk corona models.

2. RADIO OBSERVATIONS

The radio counterpart to GX 339−4 was discovered in 1994 by the Molonglo Radio Observatory, Australia (MOST), at 843 MHz (Sood & Campbell-Wilson 1994). Monitoring over subsequent years has found that the radio emission is variable, with a flux density of $\lesssim$10 mJy (Sood et al. 1997; Corbel et al. 1997; Hannikainen et al. 1998).

High-resolution 3.5 cm radio observations with the Australia Telescope Compact Array (ATCA) detected a possible jetlike feature on 1996 July 11–13 (MJD 50,275–50,277; Fender et al. 1997). An ATCA observation on 1997 Feb 3 may have a small extension in the direction opposite to this jet, but no strongly significant confirmation of the jets has been found (Corbel et al. 1997).

Figure 1 shows the daily radio spectra in 1996 July. All the data points are from ATCA, except the one at 843 MHz, which is from MOST (Hannikainen et al. 1998). The ATCA observations are the ones made at the time when the possible jetlike feature was detected; see Fender et al. (1997) for the observing details.

The radio spectrum is approximately flat, and shows a significant variability. *The spectral shape and amplitude were not anomalous for this source during the time of the possible radio jet.*

The radio emission suggests the continual presence of an outflow in this state. The approximately flat spectrum is not consistent with optically thin emission (unless the electron distribution is exceptionally hard), and indicates some absorption in the radio-emitting regions. One possible geometry would be a conical jet, such as discussed in Hjellming & Johnston (1988).

3. OSSE OBSERVATIONS AND REDUCTIONS

OSSE observed GX 339−4 as a Target of Opportunity during an outburst for 1 week beginning 1991 September 5. The OSSE flux was ∼300 mcrab between 50 and 400 keV (Grabelsky et al. 1995). A second 1 week observation was carried out beginning 1991 November 7, when the source was ∼40 times weaker (Grabelsky et al. 1995). Our observation was made 1996 July 9–23 (MJD 50,273–50,287). The flux is a factor of ∼2 lower than that found in the (brighter) 1991 September observation.

The OSSE instrument consists of four separate, nearly identical NaI–CsI phoswich detectors, with a field of view of 3°.8 × 11°.4 FWHM (see Johnson et al. 1993 and Grabelsky et al. 1995 for instrumental details and observing techniques). Our observations consist of a series of alternating on- and off-source pointings, with 2.048 minutes spent on each pointing. The on-source pointings (at $l = 339°.0$, $b = -3°.7$) were centered close to GX 339−4 ($l = 338°.9$, $b = -4°.3$), with the long dimension of the collimator oriented perpendicular to the Galactic plane. The total on-source observing time (per detector) was 1.59×10^5 s. The off-source pointings were located along the Galactic plane at ±12° from the on-source pointing (they were centered at $l = 351°.0$, $b = -3°.2$ and $l = 327°.0$, $b = -4°.1$). Both backgrounds gave the same results, indicating that there were no bright sources in either one.

Version 7.4 of the IGORE OSSE data analysis package was used to subtract the background and to generate the daily light curves and spectra in the standard way (Johnson et al. 1993). To perform joint fits with the *RXTE* spectrum, we used IGORE to generate a spectrum and response matrix that could be read by XSPEC.

Grabelsky et al. (1995) estimated the contribution from the diffuse component from the Galactic plane. They found that this is a negligible effect when the source is bright, as in our observation. The spectrum of the diffuse component also has a similar shape to that of GX 339−4. We have therefore not subtracted an estimate for the diffuse component.

We checked all of our results for the individual detectors separately and found no discrepancies. We have therefore combined all four detectors in all the results presented here.

4. DAILY LIGHT CURVES

Figure 2 shows the daily light curves for our OSSE data in the 50–70 and 70–270 keV bands, as well as the hardness ratio of these two bands. These are combined with the data from the *RXTE* ASM and BATSE Earth occultation. The BATSE light curve assumes an optically thin thermal bremsstrahlung (OTTB) model with a fixed $kT = 60$ keV (Rubin et al. 1998).

The soft X-ray flux in 1996 July was low, and the spectrum was very hard. However, unlike at the time of our Keck observation on 1996 May 12, the source was significantly detected during most of the month. During the month, the fluxes at all energies were generally rising. Figure 1 of Smith et al. (1997a) and Figure 1 of Rubin et al. (1998) show that the X-ray and gamma-ray fluxes peaked on ∼TJD 50,290.

A constant does not fit the OSSE 50–70 keV light curve. The reduced $\chi^2_\nu = 3.86$ for $\nu = 14$ degrees of freedom; the probability that a random set of data points would give a value of χ^2_ν as large or larger than this is $Q = 1.3 \times 10^{-6}$.

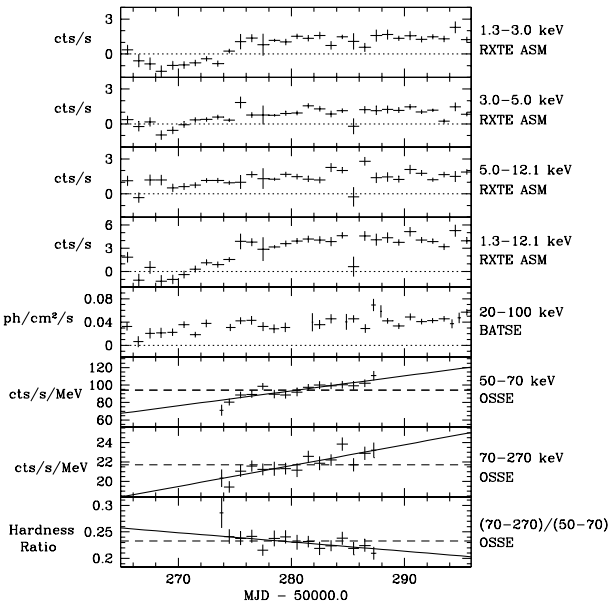

FIG. 2.—Daily light curves for 1996 July 1–31. From top to bottom, the panels are *RXTE* ASM 1.3–3.0, 3.0–5.0, 5.0–12.1, and 1.3–12.1 keV, BATSE Earth-occultation 20–100 keV (assuming a fixed OTTB model with $kT = 60$ keV), OSSE 50–70, 70–270 keV, and OSSE hardness ratio (70–270 keV)/(50–70 keV). The dashed lines show the best constant fits to the OSSE data. The solid lines show weighted least-squares linear fits to the OSSE data. The possible radio jet–like feature was seen on MJD 50,275–50,277.

Similarly, a constant also does not fit the OSSE 70–270 keV light curve with $\chi_\nu^2 = 2.88$, $\nu = 14$, $Q = 2.2 \times 10^{-4}$. For both bands, the linear relationships shown in Figure 2 give good fits ($Q = 0.35$ and 0.44, respectively).

While there is an indication from the OSSE (70–270 keV)/(50–70 keV) hardness ratio that the spectrum may be softening during the 2 week observation, this is not statistically significant. A constant fit to the hardness ratio gives acceptable results, $\chi_\nu^2 = 1.11$, $\nu = 14$, $Q = 0.34$. This fact and the linear rise in the flux are important in § 8, when we combine the nonsimultaneous *RXTE* and OSSE spectra.

Most importantly, *there was no significant change in the higher energy emission during the time when the possible radio jet–like feature was seen.* One might have expected that the physics behind the jet formation could have led to a significant change in the higher energy emission. But since the radio flux was not unusually bright during this time, it is possible that the energy release in this case was relatively small. Further multiwavelength observations during radio jet or radio flaring events will be very important to understanding whether the synchrotron-emitting electrons are involved in the Compton scattering that produces the hard X-rays. In other black hole candidates, violent changes in the high-energy emission may or may not be associated with large radio flares; e.g., GRO J1655−40 (Harmon et al. 1995; Tavani et al. 1996).

5. OSSE SPECTRA

The OSSE spectrum was extracted by averaging over the whole 2 week observation. Since the hardness ratio did not change significantly over this time, this gives a reliable measure of the spectral shape during these 2 weeks, although Figure 2 shows that the normalization on any given day will be different from the average presented here.

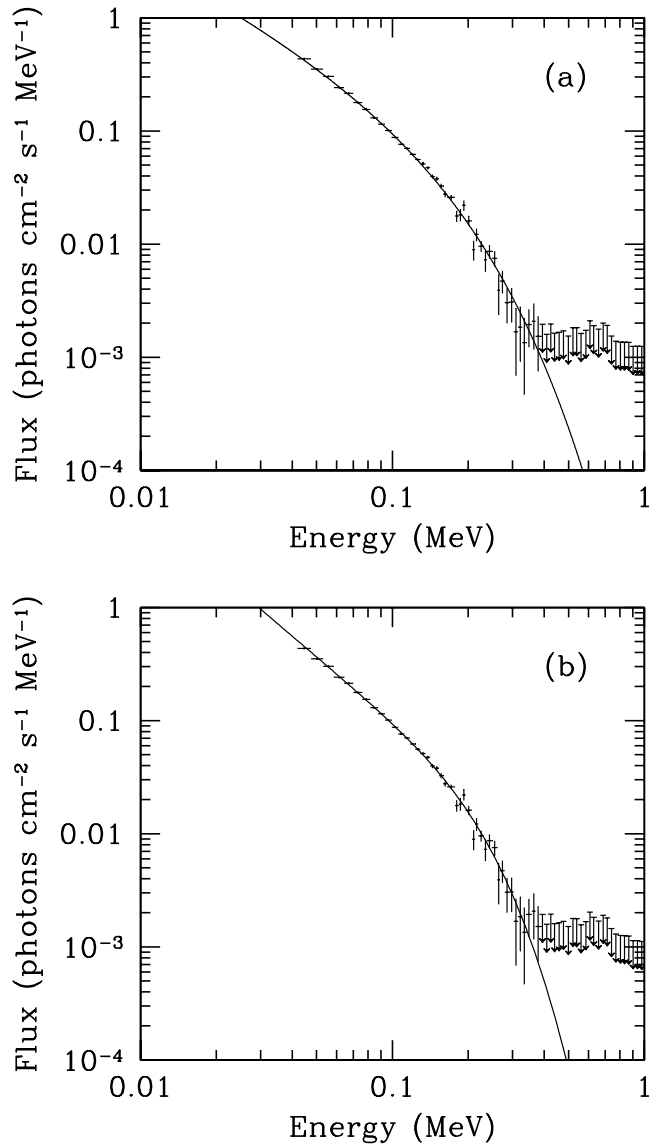

FIG. 3.—1996 July 9–23 OSSE spectrum of GX 339−4 integrated over the whole 2 week observation. (*a*) Best-fit PLE model to OSSE data alone. (*b*) Best-fit ST model to OSSE data alone. For easy comparison with Grabelsky et al. (1995), we use MeV units on both axes; all the other spectra in this paper use keV units. The upper limits are 2 σ.

The OSSE spectrum was fitted over the 0.05–10 MeV energy range using a forward-folding technique. Concerns about the OSSE instrumental response and the precision of the cross-calibration of the detectors (Grabelsky et al. 1995) are mitigated by looking at the results for the individual detectors separately. We found that the results were consistent in all four detectors, and thus we present the results for the four detectors combined.

Throughout this paper we will only consider simple phenomenological models for the spectral fitting: see Böttcher et al. (1998) for detailed self-consistent accretion disk corona model fits to all the GX 339−4 data. In the OSSE range, the spectrum has a power-law shape with a cutoff. We found that it is only necessary to use one model component to explain the OSSE spectrum, and we consider two simple functional forms:

1. Power law times exponential (PLE). In this model, the flux has the form $F(E) \propto E^{-\alpha} \exp(-E/kT)$. An optically

thin Compton spectrum can be roughly described using this model (Haardt et al. 1993).

2. Sunyaev-Titarchuk function (ST; Sunyaev & Titarchuk 1980). In this thermal Comptonization model with a spherical geometry, for energies below kT of the scattering medium the spectrum is a power law with photon index $\alpha = -(1/2) + [(9/4) + \gamma]^{1/2}$, $\gamma = \pi^2 mc^2/3kT(\tau + 2/3)^2$, and τ is the optical depth.

Figure 3 shows the best PLE and ST model fits to the OSSE data. Both functional forms give equally good fits *to the OSSE data alone.* See § 8 for the effect of doing joint fits with the *RXTE* spectrum.

The best-fit PLE model has $\alpha = 1.15 \pm 0.07$, $kT = 97 \pm 6$ keV, and a flux of 0.094 ± 0.001 photons $\mathrm{cm^{-2}\ s^{-1}\ MeV^{-1}}$ at 100 keV. (The errors are 1 σ). This has $\chi^2_\nu = 1.01$, $Q = 0.37$. The flux normalization at 100 keV is a factor of 2.0 lower than that found by Grabelsky et al. (1995) in the 1991 September observation, while our power-law index is slightly steeper (theirs was 0.88 ± 0.05), and our kT is higher (they had 68 ± 2).

The best-fit ST model has $\tau = 2.5 \pm 0.1$, $kT = 47 \pm 1$ keV, and flux 0.093 ± 0.001 photons $\mathrm{cm^{-2}\ s^{-1}\ MeV^{-1}}$ at 100 keV. This has $\chi^2_\nu = 1.00$, $Q = 0.45$. The flux normalization at 100 keV is a factor of 2.0 lower than that found by Grabelsky et al. (1995) in the 1991 September observation, while our τ is smaller (theirs was 3.0 ± 0.1), and our kT is higher (they had 37 ± 1). However, the value we derive for $\alpha = 1.9$ is the same as theirs.

Grabelsky et al. (1995) noted that their ST fit was marginal at best. They found that the model dropped off much more rapidly than the data at higher energies. As we have shown, this disagrees with our results; we get good fits to the OSSE data alone. However, in § 8 we will show that this is no longer the case when the OSSE data are combined with the *RXTE* spectrum.

6. *RXTE* OBSERVATIONS AND REDUCTIONS

The *RXTE* pointed observation was made as a Target of Opportunity on 1996 July 26 (MJD 50,290), just after the OSSE run ended. We generated the *RXTE* spectrum using two of its instruments, the Proportional Counter Array (PCA) and the High-Energy X-ray Timing Experiment (HEXTE).

The PCA consists of five Xe proportional counters, with a total effective area of about 6500 $\mathrm{cm^2}$ (Jahoda et al. 1996). These cover a scientifically validated energy range of 2–60 keV, with an energy resolution of less than 18% at 6 keV.

The HEXTE consists of two independent clusters, each containing four phoswich scintillation detectors (Rothschild et al. 1998). These have a total effective area of about 1600 $\mathrm{cm^2}$ and cover an energy range of 15–250 keV, with an energy resolution of 15% at 60 keV. Each cluster can "rock" (beam switch) along mutually orthogonal directions to provide background measurements. In our observation, the background offset was 1°.5, with a switching time of 16 s.

Both instruments have a $\sim 1°$ field of view. No other X-ray sources were in the GX 339−4 field of view or in the HEXTE background regions. For both instruments, the background dominates at higher energies. For GX 339−4, this is at $\gtrsim 70$ keV for the PCA and $\gtrsim 130$ keV for HEXTE. The PCA does not make separate background measurements. Instead, we used version 1.5 of the background-estimator program. The HEXTE background was determined from the off-source pointings in both chopping directions. For both instruments, we found that beyond the energies at which the background dominated, the model (PCA) and observed (HEXTE) background measurements were the same as what was observed in the on-source observation. This gives us confidence that the background measurements are valid. The backgrounds have been subtracted from all the spectra shown here.

For both instruments, data were only used when the spacecraft was not passing through the South Atlantic Anomaly, and when the source was observed at elevations greater than 10° above the Earth's limb and the pointing was offset less than 0°.02 from the source. The observation was short, with good data starting at 18:20:32.625 and ending at 20:14:48.497 UT. Because of the above constraints, valid data were available only in four segments: see Smith & Liang (1999) for the light curve. *We combined all these data to make one spectrum, although it should be cautioned that the source was extremely variable during this observation* (Smith & Liang 1999). For the PCA, the total on-source exposure time was 3424 s. After correcting for dead time, this gave an effective exposure of 3337 s. The dead-time correction was more important for the HEXTE data, where the time taken to rock must also be accounted for in the background exposures. For HEXTE, the adjusted on-source exposure time was 1085 s for cluster A and 1070 s for cluster B.

For the PCA, we used the Standard 2 production data set to generate the spectrum with 129 spectral channels. We used the *RXTE* tasks in FTOOLS version 4.0 to extract the data. We performed the extraction twice, once using all five Proportional Counter Units (PCUs), and once using just the top PCU layer. The top layer is responsible for $\sim 80\%$ of the detected counts, so it has the best S/N. Using all the layers gives a higher count rate, and thus a better sensitivity at higher energies, but with a lower S/N. The background contributes $\sim 13\%$ of the on-source count rate when using all the layers, and $\sim 8\%$ using just the top layer. We found that the two methods gave very similar spectral results, and we chose to retain both of them for our fitting. For both cases, we used version 2.1.2 of the PCA response matrices. We ignored the PCA data below 2 keV that are not scientifically valid. We also ignored the PCA data above 60 keV, well below the point at which the background dominated; we found that making this upper limit to the energy range smaller had no effect on the spectral fitting. We simply dropped the data around 4.78 keV, where there is a problem with the response matrix due to the Xe L edge.

For HEXTE, we used the E_8us_256_DX1F event list data. These record each individual event with 8 μs timing and 256 energy channel resolution. As with the PCA, the *RXTE* tasks in FTOOLS version 4.0 were used to extract the two HEXTE spectra, one for each cluster. For both clusters we used the 1997 March 20 versions of the HEXTE response matrices. We ignored the HEXTE data above 120 keV, well below the point at which the background dominated. We found that changing this upper limit to the energy range had no effect on the spectral fitting. Given the short exposure time, the HEXTE error bars are large, and the spectra do not extend far enough beyond the break energy to be constraining. We also ignored the HEXTE data below 20 keV. Again, this choice of energy cutoff had no effect on the fitting results.

We used the two PCA and two HEXTE spectra jointly in our spectral fitting. This was performed using XSPEC version 10.0. The relative overall normalization of the PCA and HEXTE spectra was left as a free parameter in the fitting, while all the other model parameters were the same for both instruments. We found that the relative normalization was 0.71 ± 0.01 in all the results presented here. We did not find it necessary to include separate overall normalizations between the two PCA spectra or between the two HEXTE spectra. The fitting was performed using the complete spectral resolution of both instruments, although the data have been rebinned in the figures so that each bin is at least 5 σ.

7. *RXTE* SPECTRA

As in § 5, in this paper we only consider two simplistic phenomenological models for the higher energy emission. A detailed fitting of these data using a more self-consistent model is presented elsewhere (Böttcher et al. 1998).

7.1. *Power Law Times Exponential Fit*

A PLE model fits the *RXTE* data (alone) above 15 keV. The cutoff energy is very poorly determined by the *RXTE* data, because the HEXTE error bars are large in this short observation and the *RXTE* data do not sample far beyond the cutoff energy. We therefore chose to fix $kT = 96.9$ keV at the value found for the best OSSE fit.

Figure 4 shows the results of fitting the PLE model to the data above 15 keV. This uses $\alpha = 1.26 \pm 0.01$, and a flux of 0.130 ± 0.005 photons cm^{-2} s^{-1} keV^{-1} at 1 keV. (The errors are 90% confidence regions for varying one parameter.) This has $\chi^2_\nu = 0.93$, $Q = 0.79$ (for fitting above 15 keV).

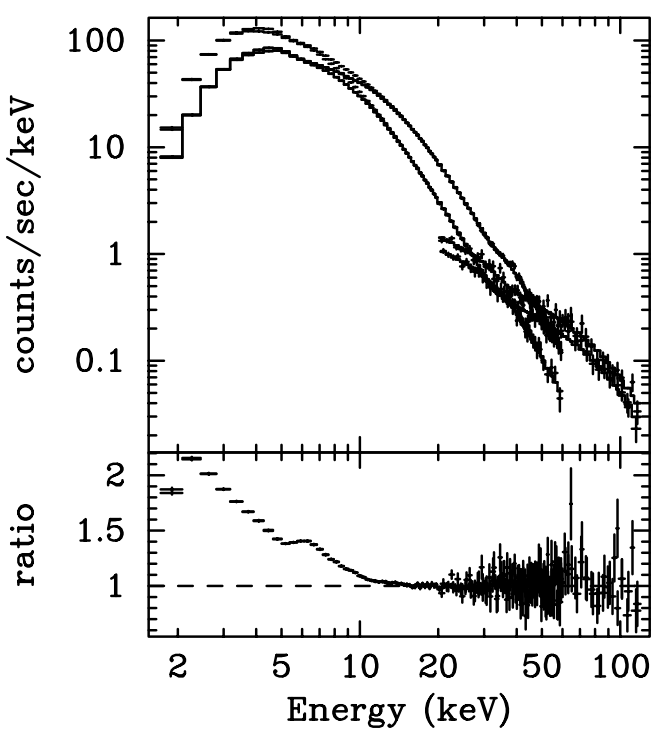

FIG. 4.—1996 July 26 *RXTE* observation of GX 339−4. PLE fit to data above 15 keV only. In all the *RXTE* figures, the top PCA curve (2–60 keV) uses all PCU, the bottom PCA curve uses just the top PCU, the top HEXTE curve (20–120 keV) is from cluster A, and the bottom HEXTE curve is from cluster B. The bottom panel plots the ratio of the data to the PLE model. Note that since this figure is for illustrative purposes, data below 2 keV and around the Xe L edge are included, although these are not used in our final fitting.

It is apparent from Figure 4 that two extra components are required to fit the spectrum at lower energies:

1. A soft component that peaks at ~2.5 keV. Such a soft component has been seen in previous GX 339−4 observations, e.g., by *Tenma* (Makishima et al. 1986), *EXOSAT* (Ilovaisky et al. 1986; Méndez & van der Klis 1997), and *Ginga* (Miyamoto et al. 1991; Ueda, Ebisawa, & Done 1994). It is present in all states, and dominates during the soft state.

2. A *broad* emission centered on ~6.4 keV. A similar feature was seen in *Ginga* observations of GX 339−4 in the low (=hard) state, and was modeled using a reflection model (Ueda et al. 1994). Using a broad iron line improved the fits in the *EXOSAT* observations of GX 339−4 made in the high (=soft) state (Ilovaisky et al. 1986). A broad line was seen in *RXTE-ASCA* observations of Cyg X-1 in the soft (=high) state (Cui et al. 1998). A very similar effect was seen in *RXTE* observations of Cyg X-1 in the low (=hard) state by Dove et al. (1998), although they chose to force the Fe Kα line to be narrow (with a line width of 100 eV, giving an equivalent width of 60 eV), which resulted in obvious residuals. *RXTE* observations of the Seyfert galaxy MCG −5-23-16 also found this feature, confirming previous *ASCA* observations (Weaver, Krolik, & Pier 1998); they interpreted it to be a broad iron line.

As we show in the next subsection, the exact form of the soft components is poorly determined by the *RXTE* data. Although we showed a data point below 2 keV in Figure 4, the PCA response matrix is currently not reliable below 2 keV, and this data point was dropped from our fitting. We therefore do not get a good measurement of the rollover, and hence cannot determine $N_{\rm H}$ reliably. Thus, for all our spectra it has been fixed at $N_{\rm H} = 5 \times 10^{21}$ cm^{-2}, as was found in the *EXOSAT* observations that more reliably measured the lower energy spectrum (Ilovaisky et al. 1986; Méndez & van der Klis 1997).

An extra broad emission feature around ~6.4 keV is always required to get a good fit. Here we assume that it is an iron-line feature that may have been broadened by orbital Doppler motions and/or scattering off a hot medium. Detailed Compton scattering line profiles have been generated using our Monte Carlo codes and are presented elsewhere (Böttcher et al. 1998). Here we simply use a broad Gaussian and an iron edge. We caution that it is possible that the broad *RXTE* feature seen in the sources listed above is due to a currently unidentified systematic flaw in the PCA response matrices, although the observations of MCG −5-23-16 make this unlikely.

Unlike the *Ginga*-OSSE observation of GX 339−4 in 1991 (Zdziarski et al. 1998), our simplistic continuum fitting of the 1996 data does not require a significant reflection component. Dove et al. (1998) found that no reflection component was needed to explain their *RXTE* observations of Cyg X-1. They noted that the broad spectral range covered by *RXTE* is an important improvement over previous observations for accurately modeling the continuum. However, we caution that we are only using simple phenomenological models in this paper; for a more self-consistent modeling of this data, see Böttcher et al. (1998), who also conclude that there is no need for a strong reflection component, because most of the incident flux from the

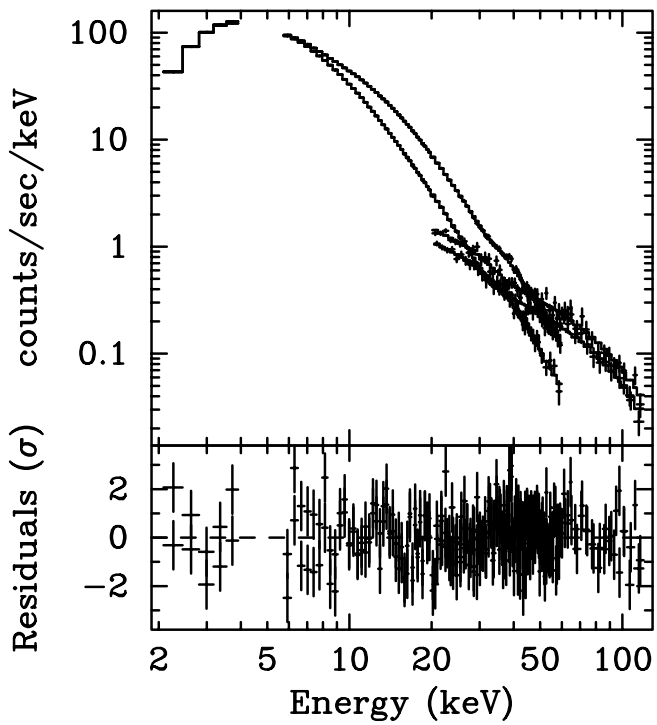

FIG. 5.—PLE model fit to 1996 July 26 *RXTE* observation of GX 339−4. The PLE component has $\alpha = 1.22 \pm 0.01$, $kT = 96.9$ keV (fixed), and flux 0.111 ± 0.005 photons cm^{-2} s^{-1} keV^{-1} at 1 keV. The soft component is a power law with photon index 3.00 ± 0.06 and flux 1.01 ± 0.05 photons cm^{-2} s^{-1} keV^{-1} at 1 keV. $N_{\rm H} = 5 \times 10^{21}$ cm^{-2} (fixed). The Gaussian line has centroid 6.6 ± 0.3 keV, width $\sigma = 1.7 \pm 0.1$ keV, and a total of 0.009 ± 0.001 photons cm^{-2} s^{-1} in the line. The edge has threshold energy 7.18 ± 0.08 keV and an absorption depth of 0.09 ± 0.02 at the threshold. The relative overall normalization of the HEXTE and PCA spectra is 0.71 ± 0.01. The errors are 90% confidence regions for varying one parameter. This fit has $\chi^2_\nu = 1.025$, $Q = 0.36$. The residuals are given in terms of σ, with error bars of size 1.

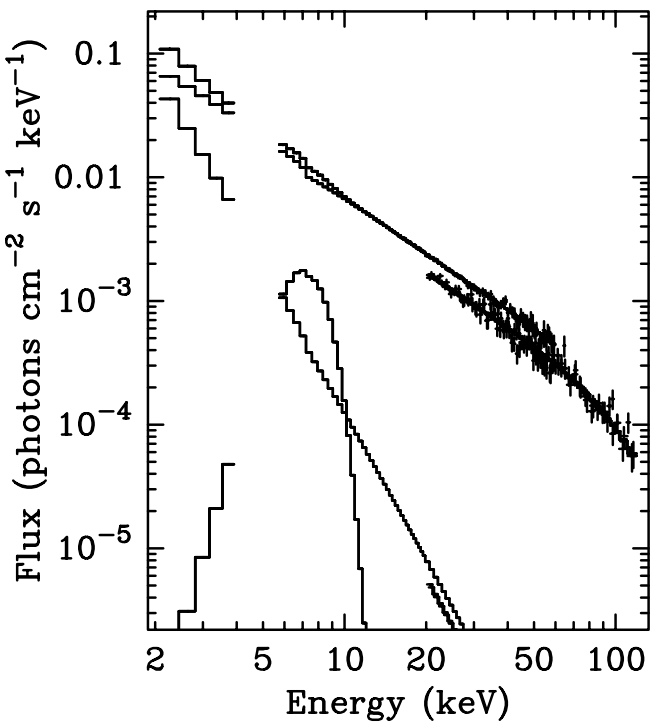

FIG. 6.—Example of ST model fit to 1996 July 26 *RXTE* observation of GX 339−4. The top curve shows the total unfolded model spectrum (not normalized), and the other curves in descending order show the hard, soft, and iron-line components. The ST component has $\tau = 4.9 \pm 0.2$ and $kT = 23 \pm 1$ keV. The ST normalization, $\kappa = 0.30 \pm 0.01$, is given by $Nf/4\pi d^2$, where N is the total number of photons from the source, d is the distance to the source, $f = z(z+3)y^z/[\Gamma(2z+4)/\Gamma(z)]$, z is the spectral index, y is the injected photon energy in units of the temperature, and Γ is the incomplete gamma function. The soft component is a power law with photon index 4.0 ± 0.1 and flux 1.3 ± 0.1 photons cm^{-2} s^{-1} keV^{-1} at 1 keV. $N_{\rm H} = 5 \times 10^{21}$ cm^{-2} (fixed). The Gaussian line has centroid 7.2 ± 0.2 keV, width $\sigma = 1.3 \pm 0.1$ keV, and a total of 0.0059 ± 0.0003 photons cm^{-2} s^{-1} in the line. The edge has threshold energy 7.12 ± 0.06 keV and absorption depth 0.14 ± 0.02 at the threshold. The relative overall normalization of the HEXTE and PCA spectra is 0.71 ± 0.01. The errors are 90% confidence regions for varying one parameter. This fit has $\chi^2_\nu = 0.99$, $Q = 0.54$.

corona goes into heating the disk surface layer and is not reflected.

Figure 5 shows an example of a complete fit to the *RXTE* data, where we have used a simple power law for the soft component. The PLE component has $\alpha = 1.22 \pm 0.01$, consistent with the OSSE best-fit value. The iron emission line is very broad. Its equivalent width (EW) is 640 eV.

7.2. *Sunyaev-Titarchuk Function Fit*

An ST model can also be used to give a good fit to the *RXTE* data *alone*. (In the next section we show that the ST model does not give a good fit to the combined *RXTE*-OSSE data.)

Figures 6, 7, and 8 show three sample fits. We show three different models for the soft component (power-law, blackbody, and thermal bremsstrahlung) to illustrate how this affects the relative contributions of the soft components. In all cases, a broad iron emission line is required. Its EW = 475, 700, and 570 eV in Figures 6–8, respectively. Note that in the unfolded spectra shown, we have not normalized the PCA and HEXTE spectra; this is discussed in the next section.

It is important to note that the spectra are very hard. *The ST component dominates the entire RXTE spectrum, even down to 2 keV*. (The PLE and soft power-law components cross at 4 keV in Fig. 5.) This is particularly important for our variability study using these data (Smith & Liang 1999), in which we divide the PCA data into three bands, 2–5, 5–10, and 10–40 keV, to try to highlight the separate components. There we show that *it is the soft 2–5 keV band that is the most variable.*

8. JOINT *RXTE*-OSSE SPECTRA

We now combine the *RXTE* and OSSE data to generate the joint spectrum. The results presented in this section should be treated with care, because the two data sets are not quite simultaneous. The fact that the OSSE hardness ratio did not change significantly over our two week observation makes it reasonable to assume that the average gamma-ray spectral shape was the same at the time of the *RXTE* observation, but this remains an assumption.

In our rapid-variability study of these *RXTE* data, we show that the hardness ratios do not change dramatically with time or brightness (Smith & Liang 1999). Thus, while the source is extremely variable, with the 2–5 keV band showing the greatest variability, the average spectra are representative of the spectral shape throughout the *RXTE* observation. However, it should be remembered that the spectrum presented here is a representative average; the

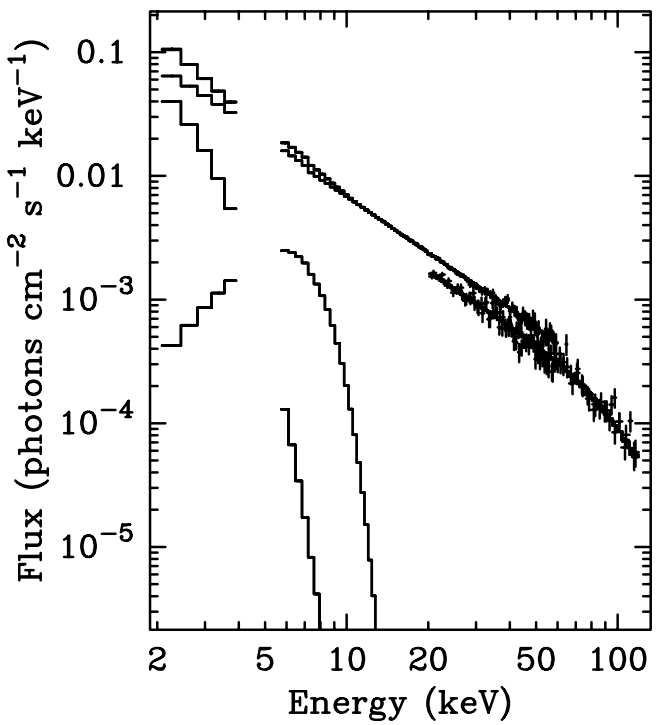

FIG. 7.—Example of ST model fit to 1996 July 26 *RXTE* observation of GX 339−4. The top curve is the total unfolded model spectrum (not normalized), and the other curves show in descending order the hard, soft, and iron-line components. The ST component has $\tau = 5.0 \pm 0.2$, $kT = 23 \pm 1$ keV, and normalization $\kappa = 0.29 \pm 0.01$. The soft component is a blackbody with $kT = 0.47 \pm 0.02$ keV and normalization $L_{39}/D_{10}^2 = 0.0069 \pm 0.0005$, where L_{39} is the blackbody luminosity in units of 10^{39} ergs s^{-1}, and D_{10} is the source distance in units of 10 kpc. Assuming a distance of 4 kpc gives $L = 1.1 \times 10^{36}$ ergs s^{-1} in the soft component. $N_{\rm H} = 5 \times 10^{21}$ cm^{-2} (fixed). The Gaussian line has centroid 5.7 ± 0.7 keV, width $\sigma = 1.9 \pm 0.3$ keV, and a total of 0.012 ± 0.003 photons cm^{-2} s^{-1} in the line. The edge has threshold energy of 7.23 ± 0.15 keV and absorption depth of 0.06 ± 0.03 at the threshold. The relative overall normalization of the HEXTE and PCA spectra is 0.71 ± 0.01. The errors are 90% confidence regions for varying one parameter. This fit has $\chi_\nu^2 = 1.19$, $Q = 0.01$.

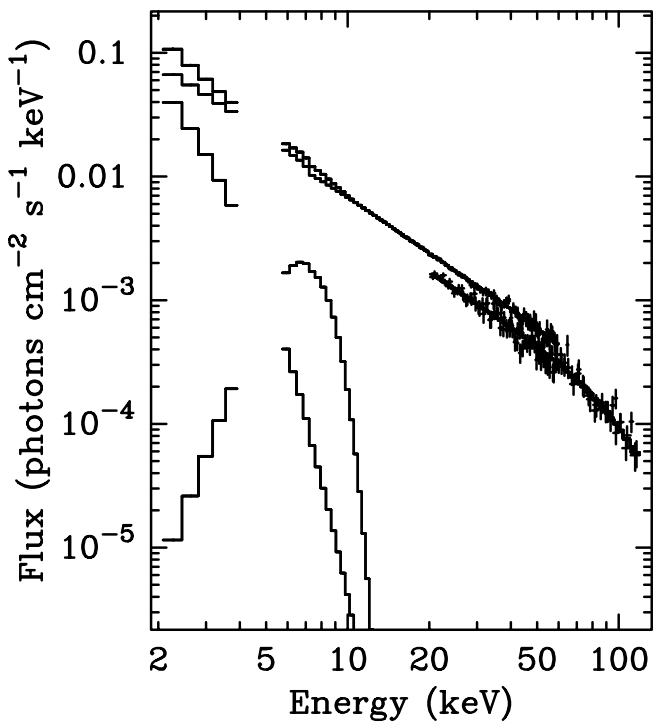

FIG. 8.—Example of ST model fit to 1996 July 26 *RXTE* observation of GX 339−4. The top curve is the total unfolded model spectrum (not normalized), and the other curves show in descending order the hard, soft, and iron-line components. The ST component has $\tau = 4.82 \pm 0.15$, $kT = 23.6 \pm 1.2$ keV, and normalization $\kappa = 0.303 \pm 0.008$. The soft component is a thermal bremsstrahlung with $kT = 1.07 \pm 0.04$ keV and normalization $[3.02 \times 10^{-15}/(4\pi D^2)] \int n_e n_I \, dV = 0.88 \pm 0.06$, where D is the source distance (in cm) and n_e and n_I are the electron and ion densities (in cm^{-3}), respectively. $N_{\rm H} = 5 \times 10^{21}$ cm^{-2} (fixed). The Gaussian line has centroid 6.8 ± 0.3 keV, width $\sigma = 1.4 \pm 0.1$ keV, and a total of 0.0075 ± 0.0006 photons cm^{-2} s^{-1} in the line. The edge has threshold energy 7.10 ± 0.07 keV and absorption depth 0.12 ± 0.03 at the threshold. The relative overall normalization of the HEXTE and PCA spectra is 0.71 ± 0.01. The errors are 90% confidence regions for varying one parameter. This fit has $\chi_\nu^2 = 1.03$, $Q = 0.31$.

actual spectrum at any given instant will have an overall normalization that can differ by a factor of ~ 3.

8.1. *Power Law Times Exponential Fit*

The PLE best fits to the separate OSSE (Fig. 3*a*) and *RXTE* (Fig. 5) data used the same $kT = 96.9$ keV and had consistent values of α. We will therefore get a good joint *RXTE*-OSSE fit provided that the relative normalizations between the different instruments can be matched. This depends on the absolute calibrations of the OSSE, PCA, and HEXTE instruments. We could simply shift the unfolded OSSE, PCA, and HEXTE spectra arbitrarily to make them match. But instead, we have used the *RXTE* ASM and BATSE data to try to be more rigorous.

The uncorrected PCA data give a 2–10 keV flux of 77 mcrab. However, the ASM gave a 2–10 keV flux of only 60 mcrab for this day. This suggests that the unfolded PCA spectrum needs to be normalized by multiplying by 0.78 to get the correct value.

The uncorrected HEXTE data give a 20–100 keV flux of 3.6×10^{-2} photons cm^{-2} s^{-1}. This is close to the BATSE measured flux of 4.0×10^{-2} photons cm^{-2} s^{-1}. This suggests that the unfolded HEXTE spectrum needs to be normalized by multiplying by 1.1 to get the correct value.

We therefore infer that the relative normalization of the HEXTE and PCA spectra should be 0.71, which is exactly what was found independently in the joint fitting.

Based on the 50–70 keV OSSE daily light curve shown in Figure 2, we would expect to have to multiply our average OSSE spectrum by a factor of $(110/94) = 1.17$ to get the correct normalization on 1996 July 26. This agrees with a joint *RXTE*-OSSE fit in XSPEC, where we get a relative normalization between OSSE and the PCA of 1.5 (which is 1.17/0.78).

Figure 9 shows the effect of shifting the unfolded spectra from Figures 3*a* and 5 by these amounts. As expected, the data sets join smoothly. The model curve is the same as in Figure 5, but with an overall normalizing factor that is 0.78 times the previous one (the *RXTE* fits assumed that the PCA was perfectly calibrated).

Figure 9 illustrates that it is extremely important that future observations of GX 339−4 should make simultaneous X-ray and gamma-ray observations in order to accurately measure the spectrum both above and below the cutoff energy.

8.2. *Sunyaev-Titarchuk Function Fit*

The ST best fits to the separate OSSE (Fig. 3*b*) and *RXTE* (Figs. 6–8) data do not give consistent ST fit param-

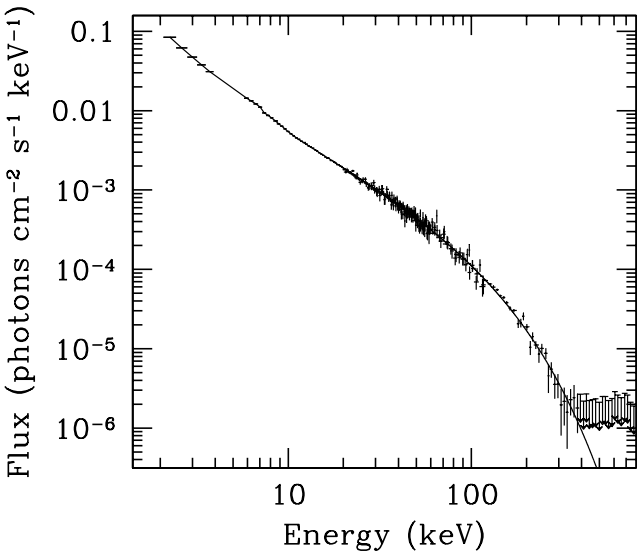

FIG. 9.—Joint *RXTE*-OSSE spectrum and PLE model fit for GX 339−4. Note that the two data sets are not quite simultaneous, and the source is highly variable, so this figure should be used with care. The PCA data from Fig. 5 have been scaled by multiplying by 0.78. The HEXTE data from Fig. 5 have been scaled by multiplying by 1.1. The OSSE data from Fig. 3*a* have been scaled by multiplying by 1.17. The model fit from Fig. 5 has been scaled by multiplying by 0.78.

eters. We therefore do not expect to get a good joint *RXTE*-OSSE fit.

Figure 10 shows the results of adding the OSSE data to Figure 6. We have fixed all the model parameters to those given in Figure 6, except for the relative normalization of the OSSE and *RXTE* instruments. It is clear that the model fit to the *RXTE* data does not explain the shape of the joint *RXTE*-OSSE spectrum; the model drops off too rapidly with increasing energies to give an acceptable joint fit. This now agrees with Grabelsky et al. (1995).

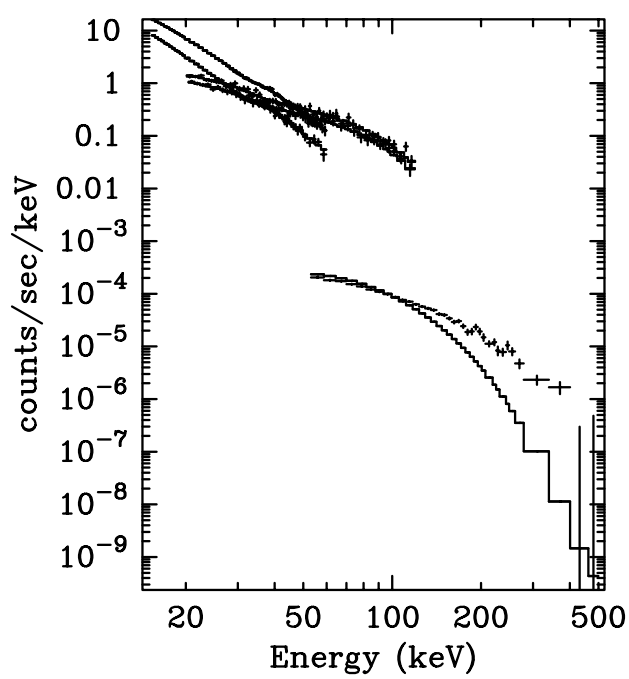

FIG. 10.—Joint *RXTE*-OSSE spectrum and ST model fit for GX 339−4. The OSSE data have been added to Fig. 6. All the model parameters are the same as in Fig. 6, with the relative normalization of the OSSE and *RXTE* instruments the only parameter that has been fitted here.

In § 5 we showed that an ST model could fit the OSSE data alone. However, we find that these model parameters do not give a good fit to the *RXTE* data. Even if we ignore all the soft components and just try to use an ST model alone to simultaneously fit the OSSE and *RXTE* data above 15 keV, we are unable to get an acceptable fit (the best $\chi^2_\nu = 1.5$, $Q = 4 \times 10^{-9}$, for $kT = 35$ keV and $\tau = 3.8$).

It is clear that the correct shape cannot be generated by the ST model when a larger energy range is available. We cannot rule out the possibility that the gamma-ray spectrum changed dramatically between the end of our OSSE observation and our *RXTE* observation, although the prior evolution of the source makes this unlikely. Again, this highlights the need for future observations of GX 339−4 to make simultaneous X-ray and gamma-ray observations.

More realistic and self-consistent Compton-scattering models can explain the harder spectrum presented here. A full study is beyond the scope of this paper, but in Böttcher et al. (1998) we develop such a detailed simulation and show that it can fit the joint GX 339−4 spectrum.

9. SUMMARY

As part of our multiwavelength campaign of observations of GX 339−4 in 1996, we present our radio, X-ray, and gamma-ray observations made in July, when the source was in a hard state (= soft X-ray low state).

The radio observations were made when there was a possible radio jet. We show that the radio spectrum was flat and significantly variable, and that the radio spectral shape and amplitude were not anomalous for the source at this time. Daily light curves from our pointed OSSE observation on July 9–23, from BATSE, and from the ASM on *RXTE*, also showed that there was no significant change in the X-ray and gamma-ray flux or hardness during the time when the radio jet–like feature was seen.

The higher energy portion of our pointed *RXTE* observation made on July 26 is equally well fitted using simple PLE and ST functions. An additional soft component is required, as well as a broad emission feature centered on ~6.4 keV. This may be an iron line that is broadened by orbital Doppler motions and/or scattering off a hot medium. Its equivalent width is ~600 eV. Both a PLE and an ST model also fit our OSSE spectrum on its own. Although the observations are not quite simultaneous, combining the *RXTE* and *CGRO* spectra, we find that the PLE model easily fits the joint spectrum. However, the ST model drops off too rapidly with increasing energies to give an acceptable joint fit.

Our results show that it is extremely important that future studies of GX 339−4 should make truly simultaneous multiwavelength observations, particularly given the variability of the source. It is essential to accurately measure the spectrum both above and below the gamma-ray cutoff energy. It will also be extremely interesting to combine future unusual radio activity with the behavior at high energies.

We thank the referee for carefully reading the manuscript and providing useful suggestions and clarifications. This work was supported by NASA grants NAG 5-1547 and NAG 5-3824 at Rice University. This work made use of the *RXTE* ASM data products provided by the ASM/*RXTE*

teams at MIT and at the *RXTE* SOF and GOF at NASA's Goddard Space Flight Center. The BATSE daily light curves were provided by the Compton Observatory Science Support Center at NASA's Goddard Space Flight Center.

REFERENCES

Böttcher, M., Liang, E. P., & Smith, I. A. 1998, A&A, 339, 87
Corbel, S., Fender, R. P., Durouchoux, P., Sood, R. K., Tzioumis, A. K., Spencer, R. E., & Campbell-Wilson, D. 1997, in AIP Conf. Proc. 410, Proceedings of the Fourth Compton Symposium, Part Two, ed. C. D. Dermer, M. S. Strickman, & J. D. Kurfess (New York: AIP), 937
Cui, W., Ebisawa, K., Dotani, T., & Kubota, A. 1998, ApJ, 493, L75
Dove, J. B., Wilms, J., Nowak, M. A., Vaughan, B. A., & Begelman, M. C. 1998, MNRAS, 298, 729
Fender, R. P., Spencer, R. E., Newell, S. J., & Tzioumis, A. K. 1997, MNRAS, 286, L29
Grabelsky, D. A., et al. 1995, ApJ, 441, 800
Haardt, F., Done, C., Matt, G., & Fabian, A. C. 1993, ApJ, 411, L95
Hannikainen, D. C., Hunstead, R. W., Campbell-Wilson, D., & Sood, R. K. 1998, A&A, 337, 460
Harmon, B. A., et al. 1995, Nature, 374, 703
Hjellming, R. M., & Johnston, K. J. 1988, ApJ, 328, 600
Ilovaisky, S. A., Chevalier, C., Motch, C., & Chiappetti, L. 1986, A&A, 164, 67
Jahoda, K., Swank, J. H., Giles, A. B., Stark, M. J., Strohmayer, T., Zhang, W., & Morgan, E. H. 1996, Proc. SPIE, 2808, 59
Johnson, W. N., et al. 1993, ApJS, 86, 693
Liang, E. P. 1998, Phys. Rep., 302, 67
Liang, E., & Narayan, R. 1997, in AIP Conf. Proc. 410, Proceedings of the Fourth Compton Symposium, Part One, ed. C. D. Dermer, M. S. Strickman, & J. D. Kurfess (New York: AIP), 461
Makishima, K., Maejima, Y., Mitsuda, K., Bradt, H. V., Remillard, R. A., Tuohy, I. R., Hoshi, R., & Nakagawa, M. 1986, ApJ, 308, 635
Méndez, M., & van der Klis, M. 1997, ApJ, 479, 926
Miyamoto, S., Kimura, K., Kitamoto, S., Dotani, T., & Ebisawa, K. 1991, ApJ, 383, 784
Poutanen, J. 1998, in Theory of Black Hole Accretion Disks, ed. J. E. Pringle & M. Abramowicz (Cambridge: Cambridge Univ. Press), in press
Rothschild, R. E., et al. 1998, ApJ, 496, 538
Rubin, B. C., Harmon, B. A., Paciesas, W. S., Robinson, C. R., Zhang, S. N., & Fishman, G. J. 1998, ApJ, 492, L67
Smith, I. A., Filippenko, A. V., & Leonard, D. C. 1999, ApJ, 519, this issue
Smith, I. A., & Liang, E. P. 1999, ApJ, 519, this issue
Smith, I. A., et al. 1997a, in AIP Conf. Proc. 410, Proceedings of the Fourth Compton Symposium, Part Two, ed. C. D. Dermer, M. S. Strickman, & J. D. Kurfess (New York: AIP), 932
———. 1997b, poster presented at the High-Energy Astrophysics Division of the AAS (Estes Park, CO, Nov. 1997)
Sood, R. K., & Campbell-Wilson, D. 1994, IAU Circ. 6006
Sood, R., Durouchoux, Ph., Campbell-Wilson, D., Vilhu, O., & Wallyn, P. 1997, in 2nd INTEGRAL Workshop: The Transparent Universe, ed. C. Winkler, T. J.-L. Courvoisier, & Ph. Durouchoux (ESA SP-382) (Nordwijk: ESA), 201
Sunyaev, R. A., & Titarchuk, L. G. 1980, A&A, 86, 121
Tavani, M., Fruchter, A., Zhang, S. N., Harmon, B. A., Hjellming, R. N., Rupen, M. P., Bailyn, C., & Livio, M. 1996, ApJ, 473, L103
Ueda, Y., Ebisawa, K., & Done, C. 1994, PASJ, 46, 107
Weaver, K. A., Krolik, J. H., & Pier, E. A. 1998, ApJ, 498, 213
Zdziarski, A. A., Poutanen, J., Mikolajewska, J., Gierlinksi, M., Ebisawa, K., & Johnson, W. N. 1998, MNRAS, 301, 435